



OPEN

## Inter-organ differences in redox imbalance and apoptosis depict metabolic resilience in migratory redheaded buntings

Anit Kumar<sup>1,4</sup>, Nitin Bhardwaj<sup>2,4</sup>, Sumit Rajaura<sup>2</sup>, Mohd Afzal<sup>3</sup> & Neelu Jain Gupta<sup>1</sup>✉

Migration, a bird's metabolic apex, depends primarily on the liver and muscle for fuel mobilization and endurance flight. In migratory redheaded buntings, adaptive increase in mitochondrial membrane (MM) proton gradient to drive ATP synthesis, measured by MM potential (MMP<sup>+</sup>) and reactive oxygen species (ROS) response, have been well characterized in the blood but not in the muscle or liver. We assessed MMP<sup>+</sup>, ROS, and apoptosis in the liver and pectoralis muscle of photosensitive nonmigratory (n Mig.) male redheaded buntings photoinduced to migratory (Mig.) states. Relative expression levels of genes associated with energy (ACADM, PEPCK, GOT2, GLUT1, and CS), ROS modulation (SIRT1), mitochondrial free-radical scavengers (SOD1, PRX4, NOS2, GPX1, and GPX4), anti-apoptotic genes (NF- $\kappa$ B), apoptotic (CASP7), and tissue damage using histology, during migration were assessed. The MMP<sup>+</sup> decreased and the ROS concentration increased, due to the metabolic load on liver and pectoralis muscle tissues during Mig. However, percentage of apoptotic cells increased in liver but decreased in muscle, which is of functional significance to migratory passerines. During Mig., in muscle, SIRT1 increased, while an increase in anti-apoptotic NF- $\kappa$ B aided immune pathway-mediated antioxidant activity and guarded against muscle oxidative damage during migration. Inter-organ differences in metabolism add to our current understanding of metabolic flexibility that supports successful migration in buntings.

Migratory songbirds use twice as much energy for their endurance flight, achieving double the metabolic rate analogous to that of similar-sized mammals<sup>1</sup>. To meet the high energy demand of migratory exercise, birds are loaded with an energy depot in the form of lipid fuel<sup>2</sup> in adipose tissue, which is twice the dry energy density<sup>3</sup>, compared to that of carbohydrates. During migratory flight, the bird liver undertakes the arduous task of breaking and mobilizing stored lipids, which has additional consequences in terms of oxidative damage<sup>4</sup>. During migration in buntings, short-chain fatty acid (SCFA) levels are increased<sup>5</sup> in blood, which also facilitates optimal oxygen demand for  $\beta$ -oxidation, as evidenced by the increased levels of fat-mobilizing enzymes<sup>1</sup>. Increased mitochondrial efficiency and decreased apoptosis counteract the redox imbalance that results from migration's increased demand for metabolites and oxygen transport<sup>6</sup>. Increases in heart size and respiratory efficiency, albeit a decrease in gastric tissue lean mass in migratory songbirds support the maintenance of metabolic and osmotic homeostasis<sup>7–10</sup>.

During migration, the liver increases in size with enhanced fatty acid synthesis<sup>11</sup>. An increase in energy demand during migration leads to fatty acid accumulation, oxidation, and hypertrophy of flight muscles<sup>12</sup>. The fat breakdown leads to oxidative stress and increased reactive oxygen species (ROS) production, as the migratory exercise progresses. Higher ROS concentrations cause oxidative damage, thus limiting bird migration<sup>13</sup>. At the cellular level, ROS, including superoxide, hydrogen peroxide, and nitric oxide, are produced in mitochondria during respiration. ROS oxidize macromolecules, causing cellular damage. On the other hand, antioxidants in cells prevent cellular damage to help survival<sup>14</sup>. During migration, birds maintain a balance between ROS production and antioxidant defense<sup>6,15</sup>.

Mitochondria (Fig. 1a) are the principal sites for energy (ATP) generation and storage. During migration in buntings, ROS increases, affecting charge on their membrane; this is measured as mitochondrial membrane

<sup>1</sup>Department of Zoology, Chaudhary Charan Singh University, Meerut 250004, India. <sup>2</sup>Department of Zoology and Environmental Science, Gurukula Kangri (Deemed to be University), Haridwar 249404, India. <sup>3</sup>Department of Chemistry, College of Science, King Saud University, 11451 Riyadh, Saudi Arabia. <sup>4</sup>These authors contributed equally: Anit Kumar and Nitin Bhardwaj. ✉email: drneelujgupta@hotmail.com

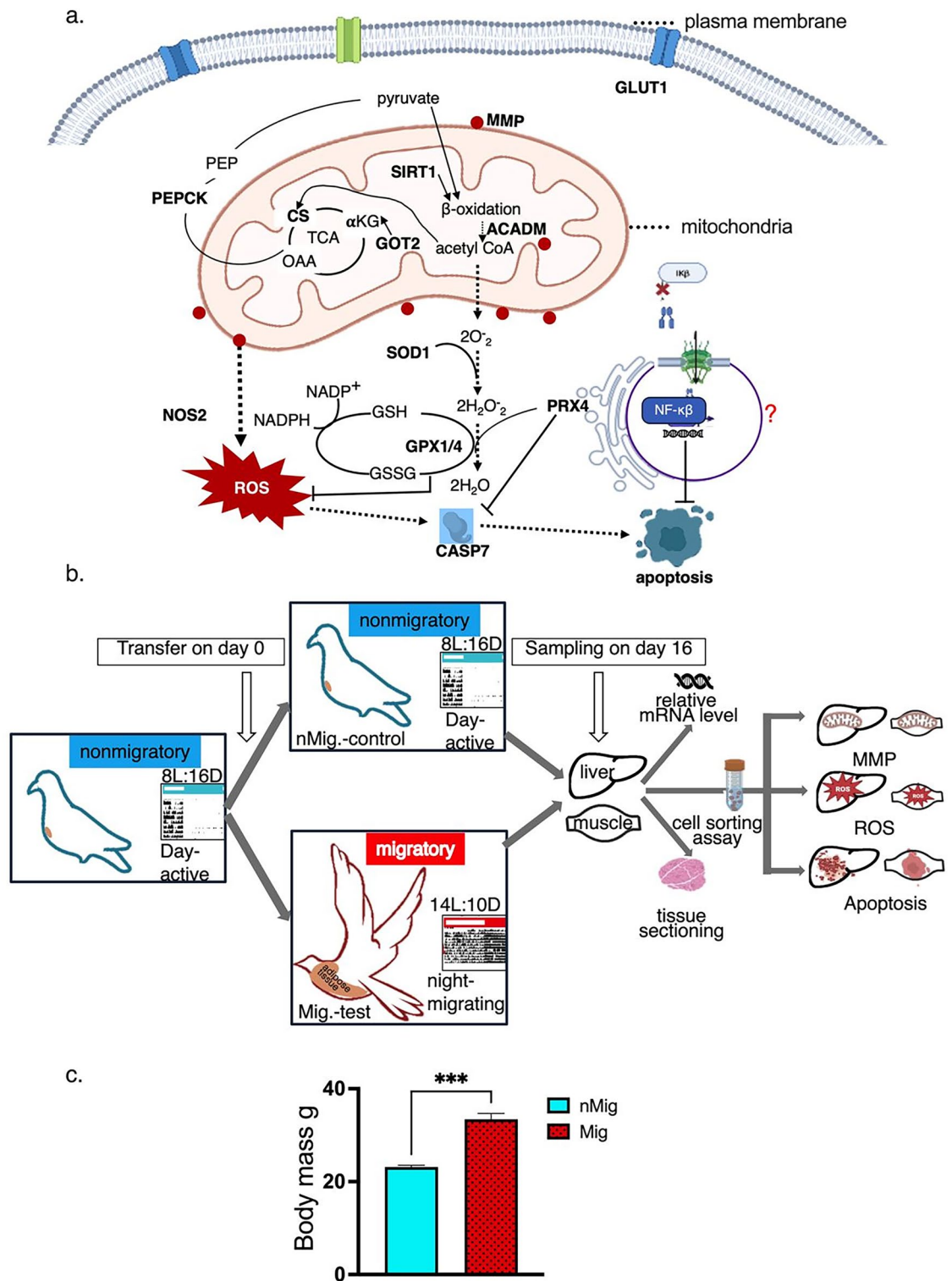


**Fig. 1.** Changes in the behaviour and physiology of nonmigratory (nMig.) and migratory (Mig.) male redheaded buntings: **(a)** schematic diagram showing genes implicated in cellular energetics, antioxidant, and immune pathways (shown in bold) affect MMP+, ROS and apoptosis inside the cell. **(b)** shows experimental design and methods. Buntings held under short days (8L:16D, cyan blue bird/bars in box, nMig., day-active, nonmigratory) and transferred to long days (14L:10D, red bird/bars in box, Mig., migratory). Open bar represents light phase, while the close bar represents dark phase. Liver and pectoral muscle tissue were collected on day 16 and either relative mRNA assay, cell sorting, or tissue sectioning was performed. Right panel shows assays for MMP+, ROS, and apoptosis in liver or muscle tissue, respectively. **(c)** Body mass differences between nMig. and Mig. groups are given in the bar graph.

potential (MMP+). Like MMP+, ROS and apoptosis in the cells are measurable when fluorescently labeled and assayed using flow cytometry. Earlier, we studied the changes in MMP+, ROS and apoptotic responses in erythrocytes during migration<sup>6</sup>. In blood, there was increase reticulocyte production occurs which indicates erythrocyte abundance. This led to higher MMP+ and lower apoptosis in migratory buntings' blood. We designed the present study to ask whether migratory birds exhibited a change in apoptosis, in liver and muscle, similar to that in blood. That is, despite extensive research on the liver and muscles of migrating songbirds, the change in mitochondrial dynamics in liver and muscles has not been investigated. With the two organs directly sustaining energy supply and flight activity execution, how the liver and muscle combat extreme oxidative stress, caused by intense migration hypermetabolism, would add to our current understanding of exercise-mediated redox imbalance and apoptosis.

Every spring, redheaded buntings (*Emberiza bruniceps*) fly from their wintering ground in India to breeding grounds in Central Asia, undertaking vernal migration. The migratory journey requires preparation, such as increased food intake to accumulate fat, thus increased body mass, hormonal changes<sup>16</sup>, and night migratory flight<sup>17,18</sup>, which can be replicated under laboratory conditions similar to those of wild conspecifics. Briefly, buntings are photosensitive (day active, hereafter, nonmigratory, nMig.) when held under short daylengths (SD) and upon exposure to long daylengths (LD), they exhibit overeating (hyperphagia), weight gain, and intense night activity within 15 days of LD exposure<sup>18</sup>. In the present investigation, we studied the role of intracellular MMP+, ROS, and apoptosis in the liver and muscle in photoinduced migrating (hereafter, migratory, Mig.) buntings to understand need-based physiological adjustment. We observed relative expression levels of pathway genes (Fig. 1a) associated with cellular energetics and relative oxidative damage in the liver and muscle in photoinduced migrating buntings, i.e., those implicated in medium chain lipid breakdown (ACADM, acyl-CoA dehydrogenase<sup>2,6</sup>), non-glucose source gluconeogenesis (PEPCK, phosphoenolpyruvate-carboxykinase<sup>19</sup>), non-glycolytic maintenance of NADPH levels (GOT2, glutamate oxaloacetate transaminase<sup>26</sup>), glucose uptake (GLUT1, glucose transporter 1<sup>20</sup>), and Krebs cycle enzyme (CS, citrate synthase<sup>19</sup>). Whether the oxidative damage-repair system of migrating buntings is equipped with the ability to remove and repair physical damage to the liver<sup>21</sup> and muscle<sup>22</sup> caused by migratory hyper-exercise was assessed by comparing the relative gene expression levels in ROS modulation (SIRT1, sirtuin1<sup>23</sup>), mitochondrial free-radical scavengers<sup>6</sup> (SOD1, superoxide dismutase<sup>6</sup>, PRX4, peroxiredoxin 4<sup>24</sup>, NOS2, nitric oxide synthase-2<sup>6</sup>, GPX1, glutathione peroxidase 1<sup>24</sup>, GPX4, glutathione peroxidase 4<sup>18</sup>), and immune genes (NF- $\kappa$ B, nuclear factor kappa B<sup>25</sup> and CASP7, caspase 7<sup>18</sup>).

## Results

### Behavioral and physiological differences between nMig. and Mig. buntings

All birds exhibited diurnal activity behavior when held under SD. In the Mig. state, the birds exhibited increased activity at night, as observed for their wild conspecifics. Buntings exhibited a 44.21% increase in body mass during the Mig. state ( $t_{10} = 7.652$ ,  $p < 0.0001$ ; Student's t test) (Fig. 1b).

### Mitochondrial dynamics in the liver and muscle from the nMig. to the Mig

In the liver (Fig. 2a–f), the daytime MMP+ decreased in the Mig. group compared to the nMig. group ( $p < 0.05$ ; Mann–Whitney test). The flow cytometry histogram representing the MMP+ cell proportion and mean fluorescence intensity (MFI) exhibited differences, with 52.5% and 581 for nMig. and 46.3% and 542 for Mig. (Fig. 2a,b). Two-way ANOVA revealed a significant decrease in the relative mRNA expression of ACADM gene (night,  $F_{(1,20)} = 5.596$ ,  $p = 0.0282$ ; day-night x nMig.–Mig. Interaction,  $F_{(1,20)} = 6.288$ ,  $p < 0.05$ , two-way ANOVA, Fig. 2c) and PEPCK (day,  $F_{(1,20)} = 7.75$ ,  $p < 0.05$ ; day-night x nMig.–Mig. Interaction,  $F_{(1,20)} = 26.04$ ,  $p < 0.001$ , two-way ANOVA, Fig. 2d) and an increase in GLUT1 gene (Mig.,  $F_{(1,20)} = 21.27$ ,  $p = 0.0002$ ), a class I facilitative glucose transporter, from the nMig. to the Mig. (Fig. 2f). No significant change was observed in the GOT2 gene expression level ( $F_{(1,20)} = 3.858$ ,  $p = 0.0635$ ) from the nMig. to the Mig. group (Fig. 2e).

In muscle (Fig. 2g–l), the daytime mean MMP+ cell percentage decreased from 95.4% in the nMig. group to 87.3% in the Mig. group ( $p = 0.0022$ ; Mann–Whitney test). The flow cytometry histogram shows that the MMP+ MFI during nMig. treatment was 754 and 311 during Mig. (Fig. 2g,h). Two-way ANOVA revealed a significant increase in PEPCK gene (Fig. 2j, day-night x nMig.–Mig. Interaction,  $F_{(1,20)} = 16.34$ ,  $p < 0.001$ , two-way ANOVA), GOT2 (Fig. 2k, night,  $F_{(1,20)} = 10.36$ ,  $p = 0.0043$ ; day-night x nMig.–Mig. Interaction,  $F_{(1,20)} = 10.46$ ,  $p < 0.005$ , two-way ANOVA), and CS gene (Fig. 2l, day,  $F_{(1,20)} = 71.13$ ,  $p < 0.0001$ , Mig.,  $F_{(1,20)} = 62.64$ ,  $p < 0.0001$ ; day-night x nMig.–Mig. Interaction,  $F_{(1,20)} = 67.61$ ,  $p < 0.0001$ ) but a decrease in ACADM (day,  $F_{(1,20)} = 4.561$ ,  $p = 0.0453$ ) from nMig. to Mig. (Fig. 2i).

### ROS production increased in liver and muscle tissue from nMig. to Mig.

In the liver (Fig. 3a–f), the daytime mean ROS + cell percentage increased from 78.1% in the nMig. group to 88.1% in the Mig. group ( $p < 0.05$ ; Mann–Whitney test). The flow cytometric histogram shows that the ROS MFI decreased from 608 in the nMig. group to 479 in the Mig. group (Fig. 3a,b). Two-way ANOVA revealed a significant increase in the expression levels of the cytosolic genes SIRT1 (Fig. 3c, night,  $F_{(1,20)} = 8.618$ ,  $p = 0.0082$ ) and SOD1 (Fig. 3d, day-night x nMig.–Mig. Interaction,  $F_{(1,20)} = 4.478$ ,  $p = 0.0471$ ) but not in NOS2 (Fig. 3e,  $F_{(1,20)} = 1.128$ ,  $p = 0.3$ ) or PRX4 (Fig. 3f,  $F_{(1,20)} = 0.8395$ ,  $p = 0.37$ ). However, remarkable day-night variation (Fig. 3e,  $F_{(1,20)} = 11.88$ ,  $p = 0.0025$ ) was observed in NOS2 during the nMig. transition.

In muscle, the daytime ROS production was greater in the Mig. group than in the nMig. group ( $p = 0.0260$ ; Mann–Whitney test). The flow cytometric histograms representing the ROS MFI during nMig. treatment were generated for 854 and 1222 during migration (Fig. 3g,h). The nighttime expression levels of the cytosolic genes SOD1 (Fig. 3j, night,  $F_{(1,20)} = 5.27$ ,  $p < 0.05$ ; day-night x nMig.–Mig. Interaction,  $F_{(1,20)} = 16.82$ ,  $p = 0.0006$ ), NOS2 (Fig. 3k, night,  $F_{(1,20)} = 89.26$ ,  $p < 0.0001$ ; day-night x nMig.–Mig. Interaction,  $F_{(1,20)} = 5.065$ ,  $p = 0.0358$ ), and

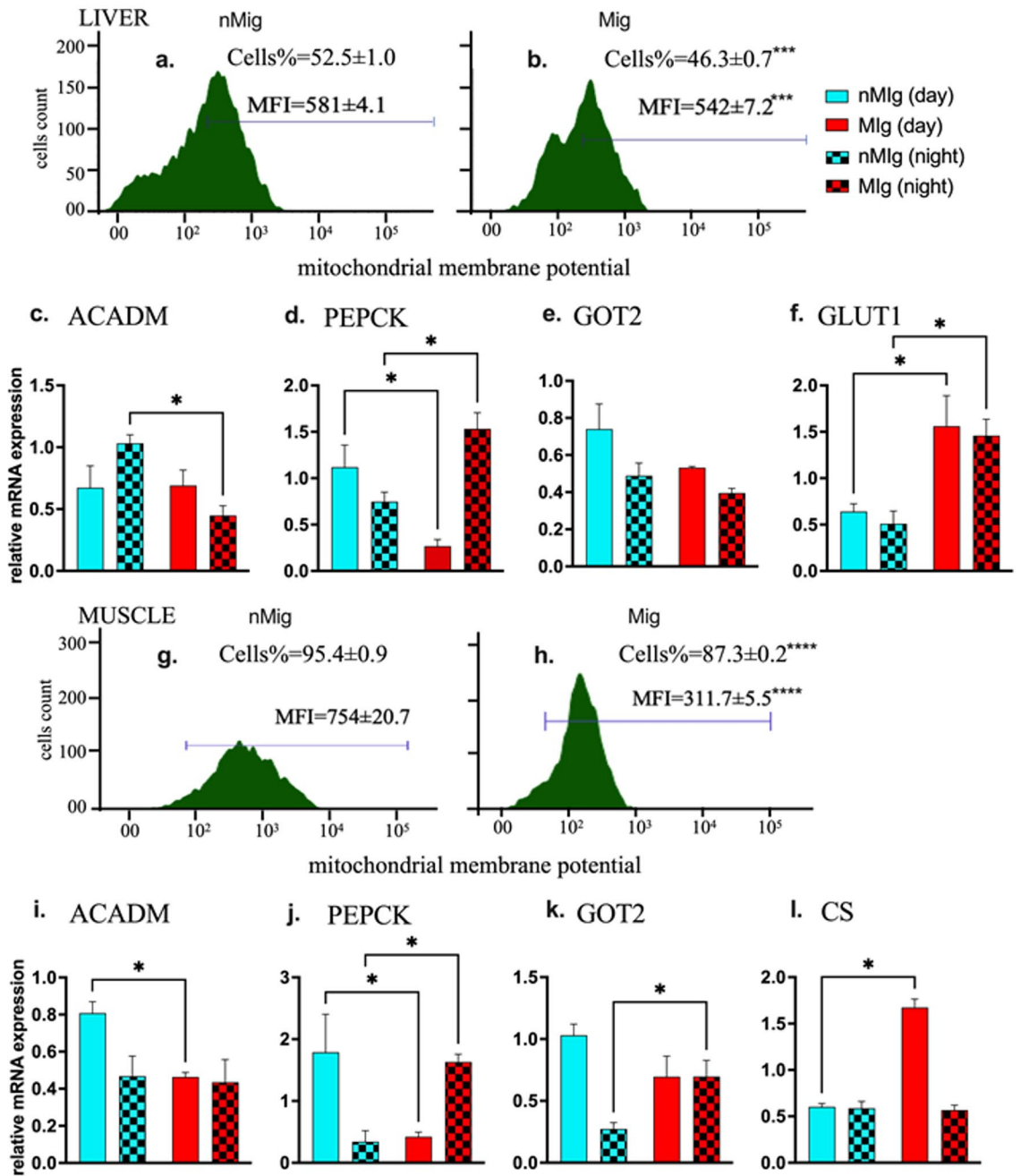


**Fig. 2.** Mitochondrial dynamics in liver and muscle from nMig. to Mig. transition. Redheaded buntings were held under SD (nMig. condition) and transferred to LD on day 0. Liver and pectoralis muscles were isolated from nMig., and Mig. buntings held on day 16. Single cell suspension was prepared, followed by MitoTracker Red staining, followed by flow cytometry analysis. The flow cytometry histogram represents mitochondrial membrane potential (MMP+) during nMig. and Mig. day in liver (a,b) and muscle (g,h), respectively. Relative mRNA expression levels of various genes in the liver and muscle were quantified by SYBR Green method. Bar graphs represent relative mRNA expression levels of ACADM, PEPCK, and GOT2 genes in liver (c–e) and muscle (i–k) during nMig. and Mig. day and night. The expression levels of GLUT1 in liver and CS in muscles have been shown in graphs (f) and (l). Bar with cyan colour is for nMig. and red for Mig.; solid and pattern bar represent day and night sampling. Horizontal bar with asterisk represents groups with significant difference ( $p < 0.05$ , Tukey’s post hoc test). Data is presented as mean ± S.E.M.  $n = 6$  in each group.

PRX4 (Fig. 3l, Mig.,  $F_{(1,20)} = 14.83$ ,  $p = 0.0010$ ) and all-time expression levels of SIRT1 (Fig. 3i, Mig.,  $F_{(1,20)} = 27.98$ ,  $p < 0.0001$ ; two-way ANOVA followed by post hoc) increased in Mig. group (Fig. 3i–l).

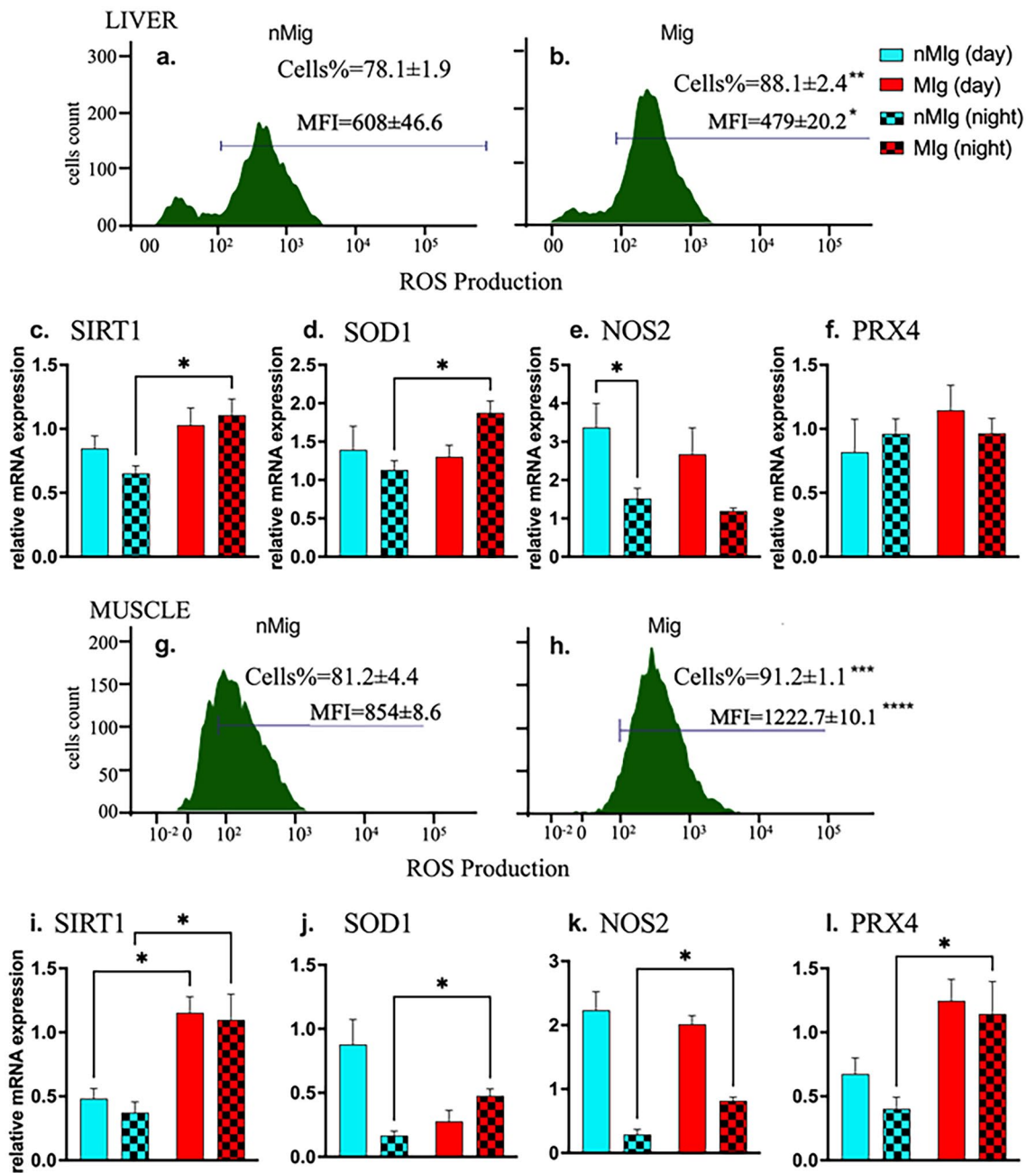


**Fig. 3.** Changes in ROS production in liver and muscle from nMig. to Mig. transition. Redheaded buntings were held under SD (nMig. condition) and transferred to LD on day 0. Liver and pectoralis muscles were isolated from nMig., and Mig. buntings held on day 16. Single-cell suspensions isolated from liver and muscles of nMig. and Mig. buntings were stained with CM-H<sub>2</sub>DCFDA stain and analysed by flow cytometry. The flow cytometry histogram represents ROS levels during nMig. and Mig. day in liver (a,b) and muscles (g,h), respectively. Relative mRNA expression levels of various genes in liver and muscle were quantified by SYBR Green method. The relative mRNA expression levels for SIRT1, SOD1, NOS2 and PRX4 in liver (c–f) and muscle (i–l) during nMig. and Mig. have been shown. Bar with cyan colour is for nMig. and red for Mig.; solid and pattern bar represent day and night sampling. Horizontal bar with asterisk represents groups with significant difference ( $p < 0.05$ , Tukey's post hoc test). Data is presented as mean  $\pm$  S.E.M.  $n = 6$  in each group.

#### Apoptosis increased in the liver but decreased in the muscles in Mig. buntings

In the liver, (Fig. 4a–h), the percentage of apoptotic cells increased ( $F_{(1,20)} = 12.18$ ,  $p < 0.005$ ) from the nMig. to the Mig. populations (Fig. 4a–d). Anti-apoptotic NF- $\kappa$ B (Fig. 4e, Mig.,  $F_{(1,20)} = 28.20$ ,  $p < 0.0001$ ) and apoptotic CASP7 (Fig. 4f, day-night x nMig.–Mig. Interaction,  $F_{(1,20)} = 24.17$ ,  $p < 0.0001$ ) decreased from nMig. to Mig. The GPX4 level increased during the night in Mig. (Fig. 4h, Mig.,  $F_{(1,20)} = 7.375$ ,  $p = 0.0133$ ), while the GPX1 level remained similar (Fig. 4g).

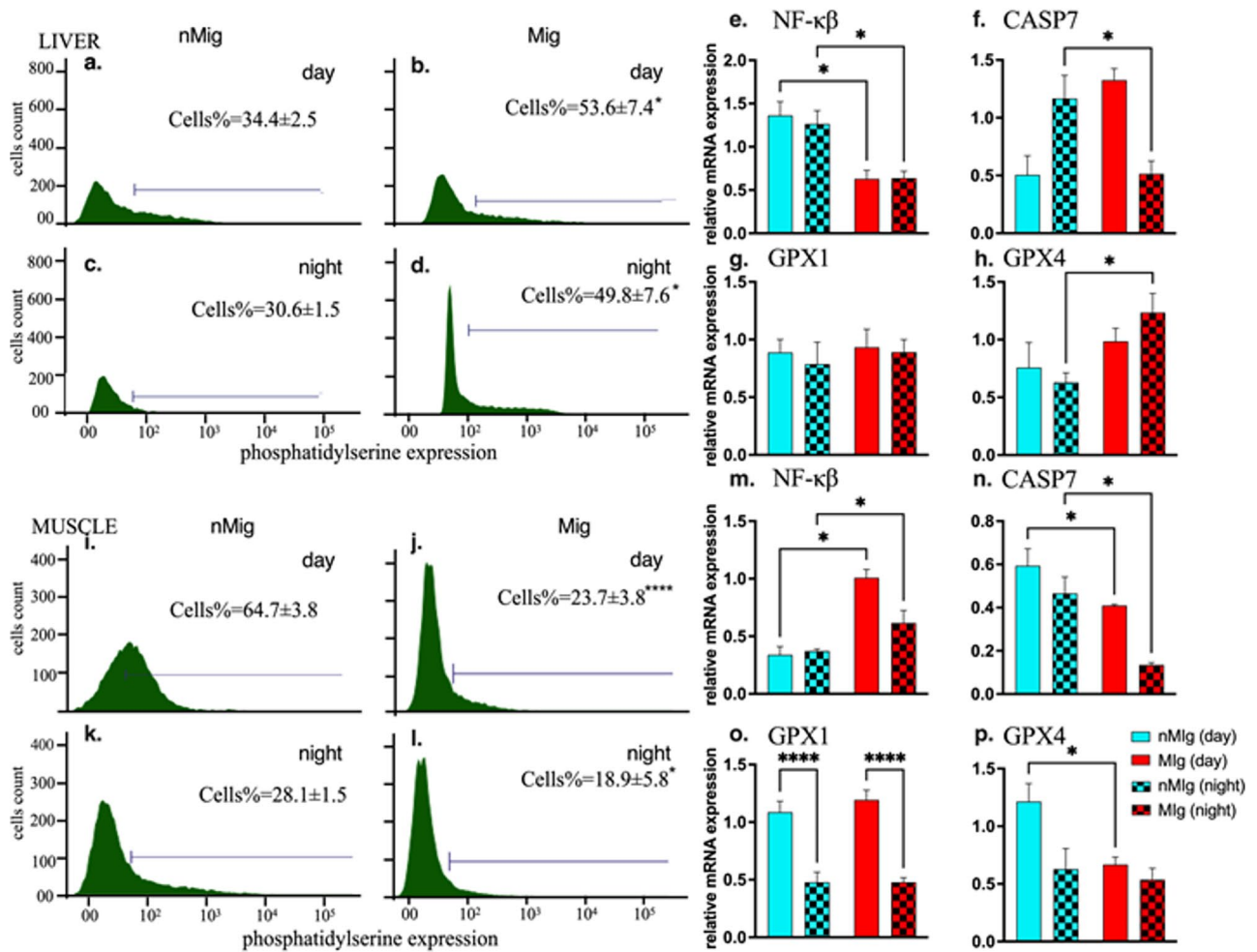


**Fig. 4.** Apoptosis increased in liver nMig. to Mig., but decreased in muscles. Redheaded buntings were held under SD (nMig. condition) and transferred to LD on day 0. Liver and muscles were isolated from nMig., and Mig. buntings held on day 16. Single-cell suspensions of liver and muscles of nMig. and Mig. buntings were stained with Annexin V antibody and analysed by flow cytometry. The flow cytometry histogram represents apoptotic cells% in nMig. and Mig. day and night in liver (a–d) and muscle (i–l), respectively. Bar diagram represents relative mRNA expression levels for NF- $\kappa$ B, CASP7, GPX1, and GPX4 in liver (e–h) and muscle (m–p) during nMig. and Mig. day and night. Bar with cyan colour is for nMig. and red for Mig.; solid and pattern bars represent day and night sampling. Horizontal bar with asterisk represents groups with significant difference ( $p < 0.05$ , Tukey’s post hoc test). Data is presented as mean  $\pm$  S.E.M.  $n = 6$  in each group.

Contrary to liver, apoptotic cell percentage in muscle (Fig. 4i–p) decreased ( $F_{(1,20)} = 38.91$ ,  $p < 0.0001$ ) from nMig. to Mig. (Fig. 4i–l). Two-way ANOVA revealed an increase in the expression levels of the anti-apoptotic gene NF- $\kappa$ B from nMig. to Mig. (Fig. 4m,  $F_{(1,20)} = 36.90$ ,  $p < 0.0001$ ) and a decrease in the expression levels of the apoptotic gene CASP7 (Fig. 4n, night,  $F_{(1,20)} = 13.38$ ,  $p < 0.005$ , Mig.,  $F_{(1,20)} = 21.93$ ,  $p = 0.0001$ ). The GPX4 level decreased from nMig. to Mig. (Fig. 4p, day,  $F_{(1,20)} = 7.47$ ,  $p < 0.05$ , Mig.,  $F_{(1,20)} = 5.9$ ,  $p < 0.05$ ), while the GPX1 level did not vary from nMig. to Mig. (Fig. 4o). Marked diurnal variation was observed in GPX1 levels among the nMig. and Mig. groups (Fig. 4o, day–night,  $F_{(1,20)} = 68.41$ ,  $p < 0.0001$ ).

#### Histopathological alterations in the liver and muscles

Liver histopathology revealed sinusoidal congestion, cytoplasmic vacuolation, and hydropic degeneration (cellular swelling due to water accumulation), along with fat droplet abundance differences in the nMig. and Mig. buntings (Fig. 5a,c). In Mig. liver, a tiny collection of kupffer cells showed apoptotic bodies and the formation of a nodule called kupffer cell microgranuloma. Muscle histopathology during nMig. and Mig. revealed swollen and fragmented myofibers with irregularly shaped macrophages. In migratory bird muscle, the accumulation of lipid droplets with inclusion bodies suggested ischemic necrosis (Fig. 5b,d).

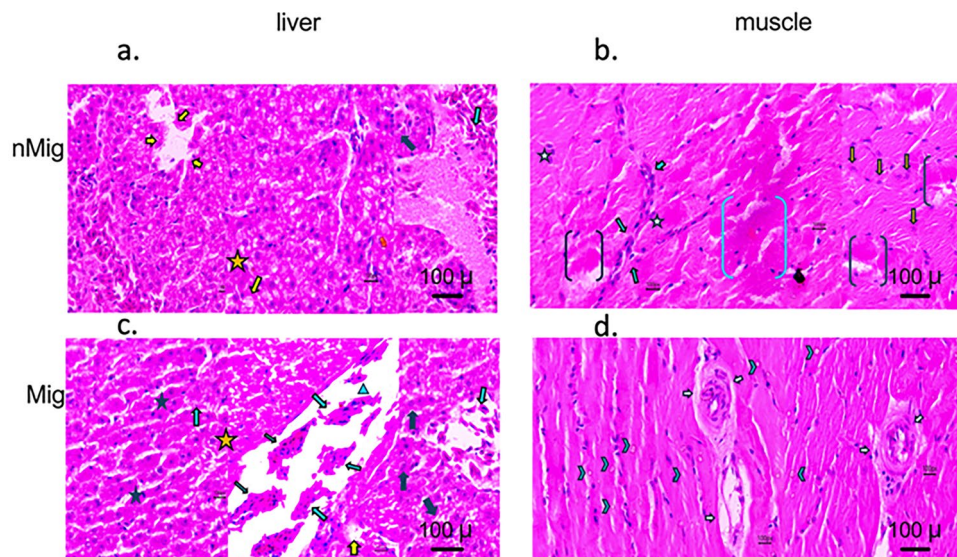


**Fig. 5.** Histopathological alterations in liver and muscles of nMig. and Mig. redheaded buntings. Redheaded buntings were held under SD (nMig. condition) and transferred to LD on day 0. Liver and muscles were isolated from nMig., and Mig. buntings held on day 16. The sections were prepared using a microtome and stained with haematoxylin and eosin. Light micrographs of the liver sections from the nMig. and Mig. have been shown in panels a and c. Panels b and d represent the histopathological alterations in pectoralis muscle in nMig. and Mig., respectively. Yellow star indicates sinusoids, cyan triangle represents hepatocytes, yellow arrow indicates apoptotic bodies, cyan star represents necrotic area, cyan arrow for macrophages, white arrow represents necrotic area in muscles, dark cyan arrow head shows lipid droplets, myofibers are shown in cyan brackets, and collagen fibers are shown in dark brackets, respectively.

## Discussion

During the high energy state of migration, the liver mediates lipid transport, combating redox fluctuations due to enhanced fatty acid mobilization<sup>26</sup> and catabolic pathways while sustaining double protein turnover compared to that in muscles<sup>27</sup>. On the other hand, muscle tissue is faced with extreme metabolic energy demands, accrued by intense contraction and relaxation<sup>28</sup>. The tissue-specific trade-off depends on the web of metabolic and immune pathways, which intersect with inflammatory and antioxidant pathways in cells. For example, during the night, in migrating European robins, GPX increases glutathione (GSH) regeneration to reduce ROS levels<sup>29</sup>. In both liver and muscle, glutamine (Gln) is taken up and deaminated to regulate the cytosolic glutamine–glutamate (Gln/Glu) redox balance and control cellular ROS through the oxidation of key molecules such as NADH/NAD<sup>+</sup><sup>30</sup>. Therefore, we expected to observe variations in  $\beta$ -oxidation and deamination in addition to changes in the level of antioxidant enzymes in the liver and muscle. DeMoranville et al.<sup>30</sup>, also showed the upregulation of several mitochondrial and fat metabolism-related genes (PPAR $\gamma$ , PGC-1 $\alpha$ , PGC-1 $\beta$ , fatty acid transporters, and oxidation) in migrating bird muscles, while only one fatty acid lysis gene was upregulated in the liver<sup>11</sup>. In our earlier study, a higher MMP+ and increased reticulocytes in blood, restrained ROS increase<sup>6</sup>, while in liver and muscle of migrating buntings, MMP+ decreased and ROS increased. Trewin et al.<sup>31</sup>, reported that extreme exercise energetic demand conditions alter mitochondrial morphology in a membrane potential-dependent manner, causing a moderate decrease in the MMP+<sup>32</sup>, which is in agreement with our findings in liver and muscle. A decline in MMP+ causes matrix condensation, releasing cytochrome c into intermembrane gaps in mitochondria, the latter leads to increase in apoptosis. Although, ROS is expected to decrease with MMP+ decline<sup>27</sup>, higher levels of ROS in migratory birds are reported<sup>29</sup>.

We observed at least a 10% increase in cellular ROS levels during migration, reaching 90% ROS levels or more, indicating the consumption of additional cellular oxygen to produce superoxide and hydrogen peroxide during the hypermetabolic state of migration. Despite similar ROS increases in the liver and muscle, liver antioxidant enzymes, except SOD1, did not exhibit significant increases during migration. In migrating bunting muscle, despite slight decrease in MMP+, resilient mitochondrial matrix activity was suggested by high mRNA expression of CS, GOT2 and PEPCK, was also observed in sparrow muscle mitochondria, which have a higher maximal rate of NADH oxidation<sup>27</sup>. This finding was confirmed by SIRT1 gene expression levels, which additionally suggested mitochondrial biogenesis during migration<sup>33,34</sup>. Interestingly, conditional antioxidant plasticity was observed in muscle during migration in buntings, albeit the relative gene expression levels might not necessarily depict enzyme levels, yet our results highlight potential inter-organ differences in mitochondrial dynamics. A concomitant increase in mRNA expression of SOD1, NOS2, and PRX4 during the night in the migratory state indicated the ability of bird muscle to sustain tissue wear and tear during intense migratory flight. This increased antioxidant capacity could also be related to reduced apoptosis in muscle (Fig. 4).

A cell's apoptotic ability, i.e., the preprogrammed cascade of self-destruction, which is essential for maintaining normal cellular homeostasis, is related to ROS levels in the tissue<sup>35</sup>. In addition to a decrease in the mRNA

expression of anti-apoptotic gene NF- $\kappa$ B of migratory bunting, there is an increase in the mRNA expression of apoptotic gene CASP7 in the liver during the day but not at night, suggesting greater apoptosis in the liver. The relative expression levels of the lipid peroxide reduction enzyme-encoding gene GPX4 also increased, suggesting that lipid peroxide accumulation in the liver could be related to ferroptosis<sup>36</sup>, which may need further investigations in birds for validation.

Decreased apoptosis in muscle in the Mig. state was similar to that in blood erythrocytes in buntings<sup>6</sup> and conformed to a similar increase in the relative expression levels of the antioxidant genes SOD1 and NOS2 in muscle and blood<sup>23</sup>. Nighttime increase in SOD1 mRNA levels in both liver and pectoralis muscle might also suggest circadian regulation of redox balance genes at night. However, this needs further investigation<sup>37</sup>. In a study on the muscles of migrating white-throated sparrows (*Zonotrichia albicollis*), Price et al. (2011) suggested that IGF1 is an important mediator of muscle phenotypic flexibility during acute exercise<sup>38</sup>. IGF1 is an inducer of NF- $\kappa$ B, the latter of which is involved in skeletal myogenesis<sup>39</sup>. A higher NF- $\kappa$ B expression level in the muscle of migrating bunting supported a decrease in apoptosis in muscle. Further, our observation of swollen and broken myofiber tissue besides inclusion bodies accumulation indicated ischemic necrosis, is in agreement with observations in Canada geese<sup>40</sup>, with the presence of lipofuscin bodies during spring migration. Our observations add to earlier suggestions<sup>22</sup> in migratory sandpipers and bar-tailed godwits, suggesting that changes in gene expression of genes associated with protection from muscle injury may not suffice to prevent muscle damage during migration in the buntings. Also, the histological indicators of muscle damage in the present study occur with Zuginruhe but without actual migratory flight. This may be taken to suggest that migratory flight may result in even more muscle damage than that documented in the present study. Migratory hyper exercise accrued necrosis in pectoralis muscle in buntings was not ruled out, yet it is for the first time that we show mechanistic details of efficient biochemical defenses against pectoralis muscle injury during migration in buntings, through increased NF- $\kappa$ B, SIRT1, SOD1, and decreased CASP7 expression levels. SIRT1 activation by acute exercise, mediates activated myogenesis<sup>33</sup>, mitochondrial biogenesis<sup>34</sup> and antioxidant function. We had similar results in Mig. state, in buntings. Imperatively, increased myogenesis and improved aerobic capacity of muscle have adaptive and functional significance for bird migration.

Our demonstration of reduced apoptosis in pectoralis muscle but not in liver tissue in migrating buntings appends our current understanding of the tissue-dependent metabolic abilities of migrating passerines. Overall, we can conclude that antioxidant activity in muscles helps prevent ROS-mediated apoptosis, which is not observed in the liver. This tissue-specific molecular metabolic flexibility<sup>41</sup> helps in the survival of redheaded buntings during spring migration.

## Methods

### Bird permission and ethical clearance

Permission to capture and work on buntings, was obtained from the Chief Wildlife Warden Rajasthan, Jaipur, India (vide F 19(02) Part File 02/CWLW/2019/1941) dated 12.03.2020. Experiment was approved by the Institutional Animal Ethics Committee (CCSU file no(s)- IAEC; IAEC/2020/02 dated- 15.12.2020, continued vide IAEC/2022/09 dated- 31.03.2022) of Chaudhary Charan Singh University, Meerut and executed in the animal house of the institution following the national guidelines and regulations of the Committee for Control and Supervision of Experiments on Animals (CCSEA), India. The study was conducted and reported in compliance with the ARRIVE guidelines.

### Birds

Redheaded buntings (*Emberiza bruniceps*) are songbirds of the Emberizidae family, showing night migration between Central Asia and South Asia. Photosensitive male buntings were captured at the wintering ground and acclimated to captivity under natural daylength (NDL) for 4 weeks, followed by acclimation to an indoor aviary under short daylength (SD) of 8 h light: 16 h dark (8L:16D, 22 ± 2 °C, 300 lx) for 2 weeks. Only male birds were used in the present study to reduce impact of reproductive physiology fluctuations. Birds (n = 36) were randomly distributed into 6 groups, where groups 1–3 (n = 18, 6 per group; effect size was taken at 2, and input was determined using g power analysis, wherein  $\alpha$  error probability was taken at 0.05 and power (1 –  $\beta$  error probability) at 0.8, rendering calculated sample size, N = 6/group) were continued under SD as controls, and groups 4–6 (n = 18, 6 per group) were transferred to long daylength (LD, 14L:10D, 22 ± 2 °C, 300 lx) on day 0 of the experiment (please also see Fig. 1b, which shows the techniques used in the study). Twelve buntings, i.e., 6 from SD (group 3) and 6 from LD (group 6), were individually housed in cages mounted with a passive infrared (PIR, DSC, LC100 PI digital PIR detector, Concord, ON, Canada) sensor for activity recording via chronobiology kit software (CK64, Stanford Software Systems USA)<sup>5,6</sup>. All photostimulated LD birds exhibited intense night activity (*Zuginruhe*), a replication of the migratory behavior of buntings in the wild. The birds were fed a mixture of foxtail millet (*Setaria italica*) supplemented with boiled eggs and water provided ad libitum. Sampling experiment design included day and night sampling for control (SD, nMig.) and test (LD, Mig.) groups, as follows. On the 16th day of the experiment, when photostimulated birds exhibited night activity, 12 birds, i.e., 6 from the SD group (group 1) and 6 from the LD group (group 4), were sampled to collect liver and muscle tissue at midday, viz. ZT4 (SD) and ZT7 (LD). The remaining 12 birds, i.e., 6 from the SD group (group 2) and 6 from the LD group (group 5) were sampled at midnight, viz. ZT16 (SD) and ZT19 (LD). As a standard method, decapitation rather than anesthesia was preferred for sampling to avoid changes in mRNA levels<sup>24,42</sup>. The liver and pectoralis muscle tissues from each bird were immediately aliquoted into three parts after collection; one was snap frozen for genomic analysis and stored in – 80 °C, the second was washed and fixed for sectioning, and the third was stored at 4 °C, in pre-labeled falcon tubes containing phosphate-buffered saline (PBS), from



which a single-cell suspension was prepared for flow cytometry (Fig. 1b). Body mass was recorded on the day of sampling for the nMig. and Mig. birds.

## Chemicals and antibodies

### *For flow cytometry assay*

5 (and 6) chloromethyl-2,7-dichlorodihydrofluorescein diacetate (CM-H<sub>2</sub>DCFDA) (C6827) was purchased from Molecular Probes, Invitrogen (Eugene, OR, USA). MitoTracker Red (MTR) (M7512) for mitochondrial membrane potential ( $\psi_m$ ) was obtained from ThermoFisher Scientific (MA, USA). Annexin V monoclonal antibodies (640907) were purchased from BioLegend (San Diego, CA, USA). RPMI medium was purchased from Sigma–Aldrich (India), and FBS was obtained from Hyclone (South Logan, UT).

### *Genomic assay*

TRIzol from Invitrogen (15,596,026; Ambion, Austin, TX, USA), RQ1 RNase-Free DNase (Promega M6101) from Promega, the RevertAid First Strand cDNA Synthesis Kit (#K1621), from Thermo Scientific™ and PCR Master Mix (K0171) from Invitrogen (Eugene, OR, USA) and PowerUp™ SYBR™ Green Master Mix (A25742) from Applied Biosystems, (Lithuania), were used. Gene-specific primers used for qPCR were made by Eurofins (Bangalore, India) and are listed in Table S1, All the other consumables were of molecular biology grade.

### *Histopathological analysis*

Liver and pectoralis muscle tissues were fixed in 10% neutral buffered formalin overnight at 4 °C and embedded in paraffin tissue block preparation. Tissue Sects. 5  $\mu$ m in thickness per slice were cut on a Leica RM2235 rotary microtome and fixed on glass slides, followed by deparaffinization and transferred onto a slide. Standard procedure for tissue dehydration and hematoxylin and eosin dichrome staining was used<sup>19</sup>. Briefly, sections were pre-treated with xylene, followed by hydration subsequently kept in haematoxylin (S014; HimMedia, Mumbai, India) for 30 s. these were further kept in ascending series of alcohol grades (100, 90, 70, 50 and 30%) and treated with Eosin (S007; HiMedia) for 1 min. before keeping. The slides containing sections were dried in absolute (100%) alcohol, cleared using xylene, and mounted underneath coverslip with DPX (18,035; Merck, Darmstadt, Germany). Sections were visualized under Axio-imager M2 semi-motorized Carl Zeiss microscope and images were captured using software ZEN 2012 (blue edition) version 1.1.0.0, Carl Zeiss Microscope GmbH.

## Flow cytometry analysis

### *Estimation of intracellular ROS and MMP+*

Liver and muscle tissues were teased into single-cell suspensions in Falcon tubes containing RPMI supplemented with 10% FBS. The suspension containing single cells with cellular debris was sieved through mesh (200  $\mu$ m) to remove cell debris, and the filtrate was pelleted by centrifugation at 1200 rpm at 4 °C followed by resuspension in RPMI medium supplemented with 10% FBS. Single-cell suspensions from the liver and muscle were suspended in prewarmed PBS supplemented with 2% FBS, and incubated with CM-H<sub>2</sub>DCFDA stain (5  $\mu$ M). CM-H<sub>2</sub>DCFDA enters cells and cleaves into non-fluorescent H<sub>2</sub>DCF. The oxidative conversion of H<sub>2</sub>DCF to its fluorescent product by ROS was measured immediately by flow cytometry<sup>43–45</sup>. The mitochondrial membrane potential was measured by staining cells with 200 nM MTR in RPMI medium for 30 min at 37 °C, followed by flow cytometric analysis<sup>46,47</sup>.

### *Apoptosis analysis*

During apoptosis, phosphatidylserine on the cell membrane flips out. Annexin V-FITC has strong binding affinity to phosphatidylserine in the presence of Ca<sup>2+</sup> ions, enabling flow cytometry assay to give a measure of apoptosis cell percentage. For apoptotic cell analysis, liver and muscle cells were suspended in PBS containing 2.5 mM calcium chloride and stained with Annexin V-FITC for 20 min at room temperature<sup>48</sup>. The cells were washed and resuspended in PBS supplemented with 2.5 mM calcium chloride (CaCl<sub>2</sub>). After incubation, the cells were washed and analyzed by flow cytometry.

All flow cytometric analysis was done on a FACSVerser flow cytometer (Becton Dickinson, USA) using FACSuite software (BD FACSuite v1.0.6). A minimum of 10,000 events (one event is the count of one cell) were analyzed for each sample using flow cytometry.

## Relative quantification of metabolic genes in liver and muscles

### *RNA isolation and preparation of cDNA*

Liver and pectoralis muscle tissue samples, stored at –80 °C. were used for this assay. These were subjected to RNA isolation using TRIzol following the manufacturer's protocol, a method used in our laboratory<sup>6</sup>. Briefly, tissue lysis was performed using a homogenizer, followed by TRIzol for cell lysis and chloroform for phase separation. The supernatant containing RNA was pelleted using propanol, washed twice with 75% ethanol, and dried. The RNA was diluted in nuclease-free water, and the concentration was measured using a Nanodrop ND2000 (Thermo Scientific™ NanoDrop™ 2000), where a 260/280 ratio of 2.0 was used to confirm the purity of the RNA. The RNA was separated on agarose gels, and the appearance of 28S and 18S rRNA bands confirmed the RNA integrity. 1  $\mu$ g RNA was used for synthesizing 20  $\mu$ L cDNA using a RevertAid First Strand cDNA synthesis kit, where the RNA was first treated with RNase-free DNase to remove DNA impurities. DNase-treated RNA was reverse transcribed into cDNA. PCR amplification (BioRad, CFX96 Touch Real-Time PCR Detection System, 30 cycles) was performed using forward and reverse primers, followed by agarose gel electrophoresis on a 1% agarose gel to confirm beta-actin amplification. PCR amplification consisted of 25  $\mu$ L reaction volume

which included 12.5  $\mu\text{L}$  of PCR Master Mix, 1  $\mu\text{L}$  each of forward and reverse primer (10  $\mu\text{M}$ ) of beta-actin, 1  $\mu\text{L}$  of template cDNA (15 ng/ $\mu\text{L}$ ) and 9.5  $\mu\text{L}$  of nuclease-free water. The amplification cycle consisted of initial denaturation (94  $^{\circ}\text{C}$  for 3 min) followed by 30 cycles of denaturation (94  $^{\circ}\text{C}$  for 1 min), annealing (55.5  $^{\circ}\text{C}$  for 1 min), extension (72  $^{\circ}\text{C}$  for 1 min) and a final extension (72  $^{\circ}\text{C}$  for 10 min).

#### Relative gene expression levels using qPCR

For qPCR, a 10  $\mu\text{L}$  reaction mixture consisted of 5  $\mu\text{L}$  of PowerUp SYBR Green, 1  $\mu\text{L}$  of each forward and reverse primer (100 nM), 1  $\mu\text{L}$  of template cDNA (15 ng/ $\mu\text{L}$ ) and 2  $\mu\text{L}$  of nuclease-free water. The amplification cycle consisted of initial denaturation (94  $^{\circ}\text{C}$  for 3 min), followed by 40 cycles of denaturation (94  $^{\circ}\text{C}$  for 10 s), annealing (60  $^{\circ}\text{C}$  for 45 s), and a final extension (72  $^{\circ}\text{C}$  for 10 min). Beta actin<sup>6</sup> was used as a reference gene, and the obtained Ct value was used to calculate relative mRNA expression levels using the formula  $\Delta\text{CT} = [\text{Ct}(\text{target}) - \text{Ct}(\text{reference})]$ , where Ct indicates threshold cycle of the target and reference genes, respectively<sup>49</sup>.  $\Delta\text{Ct}$  was normalized against  $\Delta\text{Ct}(\text{calibrator, cDNA midday} + \text{midnight for each tissue})$  to obtain  $\Delta\Delta\text{Ct}$  value. The latter was plotted as a negative exponent to 2 i.e.,  $2^{-\Delta\Delta\text{Ct}6}$ .

#### Statistical analysis

All the statistical data analyses were performed using GraphPad Prism software (version 10). The experimental design included three groups each (N = 6, per group, total 36 birds) of SD (nMig., controls) and LD (Mig., test) birds. One SD and LD group were dedicated to activity measurement, important evidence of migratory state in test group. For between-the-group comparisons, statistical significance related to relative gene levels and apoptosis was determined by two-way ANOVA followed by Tukey's post hoc analysis to determine the differences between nMig. and Mig., and day and night samples, respectively. The flow cytometry results obtained in cell%, for MMP+ and ROS, were compared for only one time point during each nMig. and Mig., therefore, we used Mann–Whitney non-parametric test. The model assumption also considered the fact, day-night differences in gene expression levels did not necessarily mirror day-night differences in MMP+, ROS, or apoptosis, therefore, causal relationships are not derived.  $p < 0.05$  was considered to indicate statistical significance. The data are presented as the mean  $\pm$  S.E.M. (standard error of the mean).

#### Data availability

Details of gene-specific primers used for qPCR, are listed in Table S1, which includes Primer sequences, GenBank accession number and related reference(s) of the previous studies in redheaded buntings, as listed in the manuscript.

Received: 24 January 2024; Accepted: 27 August 2024

Published online: 30 August 2024

#### References

- Butler, P. J. The physiological basis of bird flight. *Philos. Trans. R. Soc. Lond. B Biol. Sci.* **371**(1704), 20150384. <https://doi.org/10.1098/rstb.2015.0384> (2016).
- Guglielmo, C. G., Haunerland, N. H., Hochachka, P. W. & Williams, T. D. Seasonal dynamics of flight muscle fatty acid binding protein and catabolic enzymes in a migratory shorebird. *Am. J. Physiol. Regul. Integr. Comp. Physiol.* **282**(5), R1405–R1413. <https://doi.org/10.1152/ajpregu.00267.2001> (2002).
- Jenni, L. & Jenni-Eiermann, S. Fuel supply and metabolic constraints in migrating birds. *J. Avian Biol.* **29**(4), 521–528. <https://doi.org/10.2307/3677171> (1998).
- Skríp, M. M. & McWilliams, S. R. Oxidative balance in birds: An atoms-to-organisms-to-ecology primer for ornithologists. *J. Field Ornithol.* **87**, 1–20. <https://doi.org/10.1111/jof.12135> (2016).
- Gupta, N. J., Nanda, R. K., Das, S., Das, M. K. & Arya, R. Night migratory songbirds exhibit metabolic ability to support high aerobic capacity during migration. *ACS Omega* **5**(43), 28088–28095. <https://doi.org/10.1021/acsomega.0c03691> (2020).
- Bhardwaj, N., Kumar, A. & Gupta, N. J. Altered dynamics of mitochondria and reactive oxygen species in the erythrocytes of migrating redheaded buntings. *Front. Physiol.* **14**, 1111490. <https://doi.org/10.3389/fphys.2023.1111490> (2023).
- Guglielmo, C. G. Obese super athletes: Fat-fueled migration in birds and bats. *J. Exp. Biol.* **221**, jeb165753. <https://doi.org/10.1242/jeb.165753> (2018).
- Battley, P. F. *et al.* Empirical evidence for differential organ reductions during trans-oceanic bird flight. *Proc. R. Soc. B* **267**, 191–195. <https://doi.org/10.1098/rspb.2000.0986> (2000).
- Bauchinger, U. & McWilliams, S. Carbon turnover in tissues of a passerine bird: Allometry, isotopic clocks, and phenotypic flexibility in organ size. *Physiol. Biochem. Zool.* **82**(6), 787–797. <https://doi.org/10.1086/605548> (2009).
- Bauchinger, U., Wohlmann, A. & Biebach, H. Flexible remodeling of organ size during spring migration of the garden warbler (*Sylvia borin*). *Zoology* **108**, 97–106. <https://doi.org/10.1016/j.zool.2005.03.003> (2005).
- Araújo, P. M. *et al.* Understanding how birds rebuild fat stores during migration: Insights from an experimental study. *Sci. Rep.* **9**, 10065. <https://doi.org/10.1038/s41598-019-46487-z> (2019).
- Gutiérrez, J. S. *et al.* Oxidative status and metabolic profile in a long-lived bird preparing for extreme endurance migration. *Sci. Rep.* **9**, 17616. <https://doi.org/10.1038/s41598-019-54057-6> (2019).
- Kurutas, E. B. The importance of antioxidants which play the role in cellular response against oxidative/nitrosative stress: Current state. *Nutr. J.* **15**, 71. <https://doi.org/10.1186/s12937-016-0186-5> (2016).
- McWilliams, S. *et al.* How birds during migration maintain (oxidative) balance. *Front. Ecol. Evol.* **9**, 742642. <https://doi.org/10.3389/fevo.2021.742642> (2021).
- Jain, N. & Kumar, V. Changes in food intake, body mass, gonads and plasma concentrations of thyroxine, luteinizing hormone and testosterone in captive male buntings exposed to natural daylengths at 29° N. *J. Biosci.* **20**, 417–426 (1995).
- Jain, N. *Strategies for Endogenous Programming in the Migratory Blackheaded Bunting, Emberiza melanocephala Scopoli*. Ph. D. Thesis. (Meerut University, Meerut, 1993).
- Gupta, N. J. & Kumar, V. Testes play a role in termination but not in initiation of the spring migration in the night-migratory blackheaded bunting. *Anim. Biol.* **63**(3), 321–329. <https://doi.org/10.1163/15707563-00002415> (2013).

18. Sharma, A., Das, S., Singh, D., Rani, S. & Kumar, V. Differences in transcription regulation of diurnal metabolic support to physiologically contrasting seasonal life-history states in migratory songbirds. *J. Ornithol.* **163**, 199–212. <https://doi.org/10.1007/s10336-021-01926-5> (2022).
19. Sharma, A. & Kumar, V. Metabolic plasticity mediates differential responses to spring and autumn migrations: Evidence from gene expression levels patterns in migratory buntings. *Exp. Physiol.* **104**(12), 1841–1857. <https://doi.org/10.1113/EP087974> (2019).
20. Horton, W. J. *et al.* Transcriptome analyses of heart and liver reveal novel pathways for regulating songbird migration. *Sci. Rep.* **9**(1), 6058. <https://doi.org/10.1038/s41598-019-41252-8> (2019).
21. Guglielmo, C. G., Piersma, T. & Williams, T. D. A sport-physiological perspective on bird migration: Evidence for flight-induced muscle damage. *J. Exp. Biol.* **204**(15), 2683–2690. <https://doi.org/10.1242/jeb.204.15.2683> (2001).
22. Sharma, A. *et al.* Molecular changes associated with migratory departure from wintering areas in obligate songbird migrants. *J. Exp. Biol.* **224**(11), jeb242153. <https://doi.org/10.1242/jeb.242153> (2021).
23. Sharma, A. *et al.* Photoperiodically driven transcriptome-wide changes in the hypothalamus reveal transcriptional differences between physiologically contrasting seasonal life-history states in migratory songbirds. *Sci. Rep.* **11**(1), 12823. <https://doi.org/10.1038/s41598-021-91951-4> (2021).
24. Tiwari, J., Sur, S., Naseem, A., Rani, S. & Malik, S. Photoperiodic modulation of melatonin receptor and immune genes in migratory redheaded bunting. *Comp. Biochem. Physiol. A Mol. Integr. Physiol.* **279**, 111381. <https://doi.org/10.1016/j.cbpa.2023.111381> (2023).
25. Bairlein, F. Nutritional strategies in migratory birds. In *Avian Migration* (eds Berthold, P. *et al.*) (Springer, 2003). [https://doi.org/10.1007/978-3-662-05957-9\\_22](https://doi.org/10.1007/978-3-662-05957-9_22).
26. Elowe, C. R. & Gerson, A. R. Migratory disposition alters lean mass dynamics and protein metabolism in migratory white-throated sparrows (*Zonotrichia albicollis*). *Am. J. Physiol. Regul. Integr. Comp. Physiol.* **323**(1), R98–R109. <https://doi.org/10.1152/ajpregu.00295.2021> (2022).
27. Banerjee, S. & Chaturvedi, C. M. Migratory preparation associated alterations in pectoralis muscle biochemistry and proteome in Palearctic-Indian emberizid migratory finch, redheaded bunting, *Emberiza bruniceps*. *Comp. Biochem. Physiol. D Genom. Proteom.* **17**, 9–25. <https://doi.org/10.1016/j.cbd.2015.11.001> (2016).
28. Jenni-Eiermann, S., Jenni, L., Smith, S. & Costantini, D. Oxidative stress in endurance flight: An unconsidered factor in bird migration. *PLoS ONE* **9**(5), e97650. <https://doi.org/10.1371/journal.pone.0097650> (2014).
29. Xiao, W. & Loscalzo, J. Metabolic responses to reductive stress. *Antioxid. Redox Signal.* **32**(18), 1330–1347. <https://doi.org/10.1089/ars.2019.7803> (2019).
30. DeMoranville, K. J., Carter, W. A., Pierce, B. J. & McWilliams, S. R. Flight training in a migratory bird drives metabolic gene expression levels in the flight muscle but not liver, and dietary fat quality influences select genes. *Am. J. Physiol. Regul. Integr. Comp. Physiol.* **319**(6), R637–R652. <https://doi.org/10.1152/ajpregu.00163.2020> (2020).
31. Trewin, A. J., Berry, B. J. & Wojtovich, A. P. Exercise and mitochondrial dynamics: Keeping in shape with ROS and AMPK. *Antioxidants (Basel, Switzerland)* **7**(1), 7. <https://doi.org/10.3390/antiox7010007> (2018).
32. Picard, M., White, K. & Turnbull, D. M. Mitochondrial morphology, topology, and membrane interactions in skeletal muscle: A quantitative three-dimensional electron microscopy study. *J. Appl. Physiol.* **114**(2), 161–171. <https://doi.org/10.1152/japophysiol.01096.2012> (2013).
33. Tang, B. L. Sirt1 and the mitochondria. *Mol. Cells* **39**(2), 87–95. <https://doi.org/10.14348/molcells.2016.2318> (2016).
34. Vargas-Ortiz, K., Pérez-Vázquez, V. & Macías-Cervantes, M. H. Exercise and sirtuins: A way to mitochondrial health in skeletal muscle. *Int. J. Mol. Sci.* **20**(11), 2717. <https://doi.org/10.3390/ijms20112717> (2019).
35. Redza-Dutordoir, M. & Averill-Bates, D. A. Activation of apoptosis signaling pathways by reactive oxygen species. *Biochim. Biophys. Acta* **1863**(12), 2977–2992. <https://doi.org/10.1016/j.bbamcr.2016.09.012> (2016).
36. Bogdan, A. R., Miyazawa, M., Hashimoto, K. & Tsuji, Y. Regulators of iron homeostasis: New players in metabolism, cell death, and disease. *Trends Biochem. Sci.* **41**, 274–286. <https://doi.org/10.1016/j.tibs.2015.11.012> (2016).
37. Budkowska, M., Cecerska-Heryć, E., Marciniowska, Z., Siennicka, A. & Dołęgowska, B. The influence of circadian rhythm on the activity of oxidative stress enzymes. *Int. J. Mol. Sci.* **23**(22), 14275. <https://doi.org/10.3390/ijms232214275> (2022).
38. Price, E. R. *et al.* Migration- and exercise-induced changes to flight muscle size in migratory birds and association with IGF1 and myostatin mRNA expression levels. *J. Exp. Biol.* **214**(Pt 17), 2823–2831. <https://doi.org/10.1242/jeb.057620> (2011).
39. Bakkar, N. & Guttridge, D. C. NF-kappaB signaling: A tale of two pathways in skeletal myogenesis. *Physiol. Rev.* **90**(2), 495–511. <https://doi.org/10.1152/physrev.00040.2009> (2010).
40. George, J. C., John, T. M. & Minhas, K. J. Seasonal degenerative, reparative and regenerative ultrastructural changes in the breast muscle of the migratory Canada goose. *Cytobios* **52**, 109–126 (1987).
41. Petit, M., Clavijo-Baquet, S. & Vézina, F. Increasing winter maximal metabolic rate improves intrawinter survival in small birds. *Physiol. Biochem. Zool.* **90**(2), 166–177. <https://doi.org/10.1086/689274> (2017).
42. Staib-Laszark, I. *et al.* Anesthesia for euthanasia influences mRNA expression levels in healthy mice and after traumatic brain injury. *J. Neurotrauma* **31**(19), 1664–1671. <https://doi.org/10.1089/neu.2013.3243> (2014).
43. Bhardwaj, N. & Saxena, R. K. Elimination of young erythrocytes from blood circulation and altered erythropoietic patterns during paraquat induced anemic phase in mice. *PLoS ONE* **9**(6), e99364. <https://doi.org/10.1371/journal.pone.0099364> (2014).
44. Bhardwaj, N. & Saxena, R. K. Selective loss of younger erythrocytes from blood circulation and changes in erythropoietic patterns in bone marrow and spleen in mouse anemia induced by poly-dispersed single-walled carbon nanotubes. *Nanotoxicology* **9**(8), 1032–1040. <https://doi.org/10.3109/17435390.2014.998307> (2015).
45. Rajaura, S., Chauhan, P., Chandra, H. & Bhardwaj, N. Aflatoxin B1 administration induces reactive oxygen species production and apoptosis of erythrocytes in mice. *Toxicol.* **221**, 106963. <https://doi.org/10.1016/j.toxicol.2022.106963> (2022).
46. Bhardwaj, N. & Singh, A. Paraquat treatment modulates integrin associated protein (CD47) and basigin (CD147) expression levels and mitochondrial potential on erythroid cells in mice. *Environ. Toxicol. Pharmacol.* **58**, 37–44. <https://doi.org/10.1016/j.etap.2017.12.007> (2018).
47. Bhardwaj, N., Chauhan, P., Chandra, H., Singh, A. & Gupta, N. J. Polydispersed Acid-Functionalized Single-Walled Carbon Nanotubes Induced the Integrin-Associated Protein (CD47) and Basigin (CD147) Expression levels and Modulated the Antioxidant Gene Expression levels in Erythroid Cells in Mice. *BioNanoSci.* **13**, 695–703. <https://doi.org/10.1007/s12668-023-01071-8> (2023).
48. Bhardwaj, N., Singh, A., Chandra, H. & Gupta, K. K. Paraquat treatment modulated the stress erythropoiesis response in bone marrow and liver of the splenectomized mice. *Chem. Biol. Lett.* **9**(2), 306 (2022).
49. Livak, K. J. & Schmittgen, T. D. Analysis of relative gene expression levels data using real-time quantitative PCR and the 2<sup>(-Delta Delta C(T))</sup> method. *Methods* **25**(4), 402–408. <https://doi.org/10.1006/meth.2001.1262> (2001).

## Acknowledgements

The authors gratefully acknowledge the continued approval of the Chief Wildlife Warden Rajasthan, Jaipur, to N.J.G. (vide F 19(02) Part File 02/CWLW/2019/1941 dated 12.03.2020) to work on buntings. Financial support to N.J.G. (CRG/2019/002542) from the Science and Engineering Research Board, New Delhi, and (DEV/URGS/2022-23/49) from Chaudhary Charan Singh University is gratefully acknowledged. N.B. thanks support

from ICMR grant No. 56/2/Hae/BMS and UGC start-up grant No. 30- 496/2019. M.A. extends his appreciation to Researchers Supporting Project number (RSPD2024R979), King Saud University, Riyadh, Saudi Arabia for financial assistance. The FACS facility of the Advanced Technology Platform Centre (ATPC), managed by the Regional Centre for Biotechnology (RCB), is gratefully acknowledged.

### Author contributions

Conceived and designed the experiments: N.J.G. and N.B. Performed the experiments: A.K., S.R. and N.B. Analyzed the data: N.J.G., A.K., N.B., M.A., and S.R. Contributed reagents/materials/analysis tools: N.J.G. and N.B. Contributed to the writing of manuscript: A.K., N.J.G., N.B. M.A., and S.R. All authors reviewed the manuscript.

### Competing interests

The authors declare no competing interests.

### Additional information

**Supplementary Information** The online version contains supplementary material available at <https://doi.org/10.1038/s41598-024-71332-3>.

**Correspondence** and requests for materials should be addressed to N.J.G.

**Reprints and permissions information** is available at [www.nature.com/reprints](http://www.nature.com/reprints).

**Publisher's note** Springer Nature remains neutral with regard to jurisdictional claims in published maps and institutional affiliations.

**Open Access** This article is licensed under a Creative Commons Attribution-NonCommercial-NoDerivatives 4.0 International License, which permits any non-commercial use, sharing, distribution and reproduction in any medium or format, as long as you give appropriate credit to the original author(s) and the source, provide a link to the Creative Commons licence, and indicate if you modified the licensed material. You do not have permission under this licence to share adapted material derived from this article or parts of it. The images or other third party material in this article are included in the article's Creative Commons licence, unless indicated otherwise in a credit line to the material. If material is not included in the article's Creative Commons licence and your intended use is not permitted by statutory regulation or exceeds the permitted use, you will need to obtain permission directly from the copyright holder. To view a copy of this licence, visit <http://creativecommons.org/licenses/by-nc-nd/4.0/>.

© The Author(s) 2024